Applied Catalysis B: Environmental 224 (2018) 751–760

Contents lists available at ScienceDirect

Applied Catalysis B: Environmental

journal homepage: www.elsevier.com/locate/apcatb

Research Paper

UV–vis-infrared light-driven photothermocatalytic abatement of CO on Cu doped ramsdellite MnO_2 nanosheets enhanced by a photoactivation effect

Yi Yang, Yuanzhi Li*, Min Zeng, Mingyang Mao, Lan Lan, Huihui Liu, Jian Chen, Xiujian Zhao

State Key Laboratory of Silicate Materials for Architectures, Wuhan University of Technology,122 Luoshi Road, Wuhan 430070, PR China

A R T I C L E I N F O

Keywords:
Photocatalytic CO oxidation
Cu dope ramsdellite MnO_2
Photothermocatalytic
Photoactivation
UV–vis-infrared

A B S T R A C T

The Cu doped ramsdellite MnO_2 nanosheet samples with different Cu/Mn molar ratio were prepared by a facile hydrothermal redox reaction among $Cu(NO_3)_2$, $Mn(NO_3)_2$, and $KMnO_4$ at 60 °C. They were characterized by ICP-OES, XRD, TEM, SEM, N_2 adsorption, XPS, UV-vis-IR absorption, etc. The Cu doped ramsdellite MnO_2 nanosheet samples demonstrate highly efficient photothermocatalytic activity and very good catalytic stability for the catalytic purification of CO as one of poisonous air pollutants under the full solar spectrum infrared irradiation. Compared to the pure ramsdellite MnO_2 nanosheet sample and TiO_2(P25), the photothermocatalytic activity of the optimum Cu doped ramsdellite MnO_2 nanosheet sample under the full solar spectrum irradiation is enhanced by 2.3, 281.7 times, respectively. The Cu doped ramsdellite MnO_2 nanosheet sample also demonstrates highly efficient catalytic activity even under the $\lambda > 830$ nm infrared irradiation. The highly efficient catalytic activity of the Cu doped ramsdellite MnO_2 nanosheet sample derives from efficient solar-light-driven thermocatalysis because of its strong absorption across the entire full solar spectrum and high thermocatalytic activity. The Cu doping considerably enhances the lattice oxygen activity of ramsdellite MnO_2, thus promoting its thermocatalytic activity. A novel photoactivation, completely unlike the well-known photocatalysis on photocatalytic semiconductors such as TiO_2, is discovered to further enhance the solar-light-driven thermocatalytic activity. We combine the experimental evidence of CO-TPR and DFT calculation to reveal the origin of the novel photoactivation: the irradiation considerably enhances the lattice oxygen activity of the Cu doped ramsdellite MnO_2 nanosheets, thus accelerating their solar-light-driven thermocatalytic activity.

1. Introduction

Utilizing the clean and inexhaustible solar energy for the purification of pollutants based on various photocatalysts has attracted a lot of attention for decades. However, most of the reported photocatalysts can only utilize the UV or part of visible light [1–3]. Hence, expanding the photocatalytic response to the infrared region, which accounts for ~50% of full solar spectrum energy, is crucial and great challenging. Several strategies have been reported for developing infrared photocatalysts [4]. One strategy is to synthesize narrow bandgap photocatalysts so that the photocatalyst can be excited by near-infrared light. The near-infrared photocatalysts involve Bi_2WO_6/TiO_2 [5], $BiErWO_6$ [6], Bi_2MO_6 (M = W, Mo) [7], $Cu_2(OH)PO_4$ [8,9], WS_2 [10], PbSe/CdSe/CdS [11], Ag_2O [12], etc. Another strategy is to prepare nanocomposites of UV or visible photocatalysts with different upconversion materials (e.g. rare earth metal ions, carbon quantum dots) which convert infrared light to UV or visible light. The near-infrared upconversion photocatalysts involve $NaYF_4$:Yb,Tm/CdS [13], $YF_3:Yb^{3+},Tm^{3+}/TiO_2$ [14,15], Er^{3+}/Yb^{3+} codoped $CaF_2@TiO_2$ [16], $NaYF_4:Yb^{3+},Tm^{3+}/Er^{3+}@SiO_2@TiO_2$ [17], carbon quantum dots/TiO_2 [18], carbon quantum dots/Cu_2O [19], etc. The third strategy is to prepare near-infrared plasmonic photocatalysts which utilize plasmonic hot electrons for photocatalytic reactions. The near-infrared plasmonic photocatalysts involve $Cu_7S_4@Pd$ [20], Au/TiO_2 [21], Pt-modified Au nanorods [22], Au/$BiVO_4$ [23], etc. The above near-infrared photocatalysts were generally designed according to the well-known photocatalytic principle of redox reaction induced by electrons and holes photogenerated on the photocatalysts. Most of them have been reported to exhibit photocatalytic activity with near-infrared irradiation for the photodegradation of water pollutants such as dyes. There have been few reports about near-infrared photocatalysts for the photocatalytic purification of air pollutants such as volatile organic compounds (VOCs), CO, etc.

Recently, our group and several other groups have developed diverse photothermocatalysts to exhibit catalytic activity and very good catalytic stability for the purification of air pollutants under the full

* Corresponding author.
E-mail addresses: liyuanzhi66@hotmail.com, liyuanzhi@whut.edu.cn (Y. Li).

https://doi.org/10.1016/j.apcatb.2017.11.017
Received 8 June 2017; Received in revised form 5 September 2017; Accepted 8 November 2017
Available online 11 November 2017

solar spectrum or infrared irradiation [24–33]. The photothermocatalysts, which are designed according to solar-light-driven thermocatalytic principle, involve manganese oxide [24,25] and its nanocomposites (such as MnO_x/TiO_2, $CeMn_xO_y/TiO_2$, MnO_x-CeO_2) [26–29], $Ce_{1-x}Bi_xO_{2-\delta}$[30], Co_3O_4 [31], Pt/$LaVO_4/TiO_2$ [32], Pt/CeO_2 [33], etc. Among the photothermocatalysts, manganese oxide and its nanocomposites are much attractive due to their excellent infrared photothermocatalytic performance, inexpensiveness, earth-abundance, and environmental benignity. It is highly desirable to develop novel approach to further enhance their photothermocatalytic performance.

Ramsdellite MnO_2 is one polymorph of manganese oxide. Recently, we reported that ramsdellite MnO_2 nanosheets demonstrated highly efficient photothermocatalytic activity for the purification of benzene under the full solar spectrum, visible-infrared, or infrared irradiation [34]. Herein, we prepared the Cu doped ramsdellite MnO_2 nanosheet samples with different Cu/Mn molar ratio by a facile hydrothermal redox method. It is found that the Cu doping significantly enhances the photothermocatalytic activity of ramsdellite MnO_2 for the catalytic purification of CO as one of poisonous air pollutants under the full solar spectrum irradiation with a relatively low light intensity (about one sun), which is attributed to a considerable enhancement in its lattice oxygen activity upon the Cu doping. The Cu doped ramsdellite MnO_2 nanosheet sample also demonstrates highly efficient catalytic activity under the visible-infrared or infrared irradiation. The highly efficient catalytic activity of the Cu doped ramsdellite MnO_2 nanosheet sample is attributed to its strong absorption across the entire full solar spectrum and high thermocatalytic activity, which result in efficient solar-light-driven thermocatalytic oxidation of CO. A novel photoactivation, completely unlike the well-known photocatalysis on photocatalytic semiconductors such as TiO_2, is discovered to further promote the solar-light-driven thermocatalytic activity. We reveal the origin of the novel photoactivation by combining the experimental evidence of CO-TPR and DFT calculation.

2. Experimental section

2.1. Preparation

Cu doped ramsdellite MnO_2 samples with different Cu/Mn molar ratio were prepared according to the procedure as follows: 14.316 g of 50 wt% $Mn(NO_3)_2$ solution was added into 100 mL of distilled water in a 200 mL beaker under stirring. 0.9060 g of $Cu(NO_3)_2{\cdot}3H_2O$ was added to the $Mn(NO_3)_2$ aqueous solution under stirring until it was dissolved. Subsequently, 3.1608 g of $KMnO_4$ was added to the mixed solution of $Mn(NO_3)_2$ and $Cu(NO_3)_2$ under stirring. The beaker, which was covered with polyethylene film, was placed in an electric oven and kept at 60 °C for 12 h. The obtained precipitant was washed with distilled water and dried at 60 °C overnight. The obtained Cu doped ramsdellite MnO_2 sample was denoted as Cu-RM-A.

The other Cu doped ramsdellite MnO_2 samples with higher Cu/Mn molar ratio were prepared with the same procedure as that of Cu-RM-A except for the addition of 1.8120 or 3.6240 g of $Cu(NO_3)_2{\cdot}3H_2O$. The obtained Cu doped ramsdellite MnO_2 samples were denoted as Cu-RM-B, Cu-RM-C, respectively.

The pure ramsdellite MnO_2 sample (R-MnO_2) was prepared with the same procedure as that of Cu-RM-A except for no addition of $Cu(NO_3)_2{\cdot}3H_2O$ described in our previous work [34].

2.2. Characterization

The chemical composition of the Cu doped ramsdellite MnO_2 samples was determined by a Prodigy 7 inductively coupled plasma-optical emission spectroscopy (ICP-OES). Their X-ray diffraction (XRD) patterns were obtained on a RigakuDmax X-ray diffractometer. Their morphology was characterized by TEM and SEM on a JEM-100CX electron microscope and an ULTRA PLUS-43-13 scanning electron microscope, respectively. Their BET surface area was measured by using N_2 adsorption at −196 °C on a physisorption instrument (Micromeritics ASAP2020). Their XPS spectra were recorded on an ESCALAB 250Xi X-ray photoelectron spectrometer with Mg Kα radiation. UV–vis-IR absorption spectra were recorded on a Lambda 750 S spectrophotometer.

CO temperature programmed reduction (CO-TPR) of the Cu doped ramsdellite MnO_2 samples was conducted in a quartz tube reactor with a quartz window linked at one end of the reactor on TP5080 multifunctional adsorption apparatus. 0.0100 g of the sample supported on quartz wool was put in the quartz tube reactor. 5 vol% CO/He was fed into the reactor. In order to investigate the effect of the irradiation on the CO-TPR of the Cu doped ramsdellite MnO_2 sample, a 500 W Xe lamp (CHF-XM500) as a simulated solar light source was turned on. In this case, the amount of the sample is 0.0050 g. The light intensity is 92.3 mW cm^{-2}. The experimental details were described in our previous work [34].

2.3. Photothermocatalytic and photocatalytic activity

The photothermocatalytic activity of the Cu doped ramsdellite MnO_2 samples for the catalytic oxidation of CO under the irradiation of the Xe lamp was measured under steady state on a cylindrical reaction reactor with a quartz window. 0.1000 g of the sample coated on a slice of aluminum silicate fiber for thermal insulation was placed on the bottom of the reactor. A feed stream with 15 g m^{-3} of CO, produced by mixing 5 vol% CO/He and 20.8 vol% O_2/N_2, was continuously fed into the reactor with a flow rate of 20 mL min^{-1} (the corresponding space velocity: 12000 mL g^{-1} h^{-1}). The concentration of CO and the produced CO_2 was analyzed by a GC9560 gas chromatograph. In order to measure the photothermocatalytic activity of the Cu doped ramsdellite MnO_2 samples under the visible-infrared or infrared irradiation from the Xe lamp, a long-wave pass cutoff filter of 420, 480, 560, 690, or 830 nm was placed in the front of the quartz window of the reactor. The light intensity of the irradiation of $\lambda >$ 420, 480, 560, 690, and 830 nm is 98.4, 95.9, 93.1, 91.5, and 96.4 mW cm^{-2} respectively. The experimental details were reported in our previous work [25].

In order to measure the photocatalytic activity of the Cu doped ramsdellite MnO_2 sample for the catalytic oxidation of CO under the irradiation of the Xe lamp, 0.1000 g of the sample was coated on a glass slide. The reactor was placed in an ice-water bath to maintain the temperature at near ambient temperature under the irradiation of the Xe lamp. The other procedure was the same as that for measuring the photothermocatalytic activity.

2.4. Thermocatalytic and photothermocatalytic activity at the different temperature

The thermocatalytic activity of the Cu doped ramsdellite MnO_2 samples for the catalytic oxidation of CO at different temperature in the dark was measured under steady state in a quartz tube reactor with a quartz window linked at one end of the reactor on a gas-phase reaction apparatus (WFS-2015). 0.0500 g of the sample supported by quartz wool was placed in the reactor. A feed stream with 12.5 g m^{-3} of CO, produced by mixing 5 vol% CO/He and 20.8 vol% O_2/N_2, was continuously fed into the reactor with a flow rate of 20 mL min^{-1}.

In order to investigate the effect of the irradiation on the thermocatalytic activity of the Cu doped ramsdellite MnO_2 sample at different temperature, the Xe lamp, which was placed in the front of the window of the quartz tube reactor, was turned on. In this case, the amount of the Cu doped ramsdellite MnO_2 sample is 0.0125 g. The light intensity is 96.3 mW cm^{-2}. The experimental details were provided in our previous work [35].

2.5. DFT calculation method

Density functional theory (DFT) calculations by utilizing the Perdew–Burke–Ernzerhof functional and Projected Augmented Wave (PAW) pseudopotentials [36,37] embedded in the Vienna Ab-initio Simulation Package (VASP 5.3) were conducted to investigate the Cu doped ramsdellite MnO_2. DFT + U method with Mn3d U^{eff} (3.9 eV) and Cu3d U^{eff} (3.0 eV) [35,38,39] was utilized to introduce orbital-dependent corrections for the strong on-site Coulomb repulsion among the localized 3d electrons of Mn and Cu. A 2 × 2 × 2 Monkhorst-Pack k-point mesh was used for summations over the Brillouin zone. The convergence criteria for the electronic relaxation was 10^{-4} eV, and the convergence criteria for the ionic relaxation was 10^{-3} eV Å^{-1}.

3. Results and discussion

3.1. Preparation and characterization

The Cu doped ramsdellite MnO_2 samples with different Cu/Mn molar ratio were prepared by a facile hydrothermal redox reaction among $Cu(NO_3)_2$, $Mn(NO_3)_2$, and $KMnO_4$ (Experimental). The Cu doped ramsdellite MnO_2 samples are denoted as Cu-RM-A, Cu-RM-B, Cu-RM-C respectively. For comparison, pure ramsdellite MnO_2 sample was prepared. The chemical composition of the Cu doped ramsdellite MnO_2 samples is determined by ICP-OES. As shown in Table 1, the Cu/Mn molar ratio of Cu-RM-A, Cu-RM-B, and Cu-RM-C is 0.0037, 0.0076, and 0.0120, respectively. The result indicates that a small amount of Cu ions is doped into the MnO_2 samples. The crystalline structure of the Cu doped ramsdellite MnO_2 samples is determined by XRD. As shown in Fig. 1, the XRD peaks of all the Cu doped MnO_2 samples can be indexed to those of pure orthorhombic ramsdellite MnO_2 (JCPD 44-0142), indicating that the Cu doping does not alter their crystalline structure. The morphology of the Cu doped ramsdellite MnO_2 samples is characterized by SEM. The Cu doped ramsdellite MnO_2 samples have similar morphology of closely connected nanosheets with size of several hundred nanometers and thickness of tens of nanometers as shown in Fig. 2. The observation suggests that the Cu doping does not alter their morphology of nanosheets. Their morphology is further characterized by TEM. TEM images confirm that the Cu doped ramsdellite MnO_2 samples have similar morphology of closely connected nanosheets. HRTEM image on the side of a nanosheet for the Cu doped ramsdellite MnO_2 samples demonstrates that the nanosheet side has lattice spacing of 0.47 nm corresponding to {200} facets (Fig. 3).

The Cu doped ramsdellite MnO_2 samples is characterized by N_2 adsorption/desorption (Fig. S1). The BET surface area of Cu-RM-A, Cu-RM-B, and Cu-RM-C is 67.6, 76.5, and 97.3 $m^2\ g^{-1}$, respectively. Their BJH N_2 adsorption pore volume is 0.40, 0.48, 0.46 $cm^3\ g^{-1}$, respectively (Table 1).

The valence state of Cu and Mn in the Cu doped ramsdellite MnO_2 samples is determined by analyzing their XPS spectra (Fig. 4). Fig. 4A shows the Cu 2p spectra of the Cu ramsdellite MnO_2 samples. All the Cu ramsdellite MnO_2 samples demonstrate two weak peaks around ~933.3 and ~953.5 eV, which are attributed to Cu 2p3/2 and Cu 2p1/2 of Cu^{2+} [35,40]. With the increase of Cu/Mn molar ratio, the two peaks are intensified. All the Cu doped ramsdellite MnO_2 samples demonstrate strong peak around ~946.1 eV, which is attributed to the satellite peak of Cu^{2+} [35,40].The result suggests that Cu exists in the form of Cu^{2+} in all the Cu doped ramsdellite MnO_2 samples.

Table 1
The chemical composition, BET surface area, pore volume, Mn^{3+}/Mn^{4+} atomic ratio of the Cu doped MnO_2 samples.

Sample	Cu/Mn by ICP	N_2 adsorption/desorption		XPS		
		Surface area ($m^2\ g^{-1}$)	pore volume ($cm^3\ g^{-1}$)	Mn^{3+}/Mn^{4+} by Mn2p	AOS by Mn^{3+}/Mn^{4+}	AOS by Mn3s
Cu-RM-A	0.0037	67.6	0.40	1.64	3.38	3.42
Cu-RM-B	0.0076	76.5	0.48	1.82	3.35	3.40
Cu-RM-C	0.0120	97.3	0.46	2.08	3.32	3.37

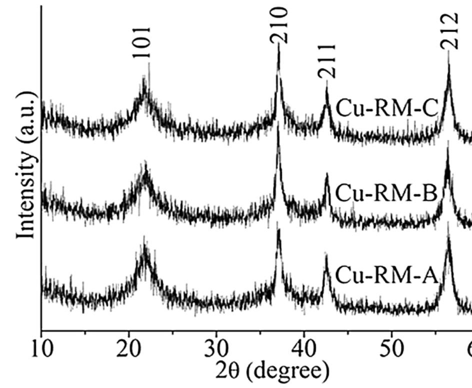

Fig. 1. XRD patterns of the Cu doped MnO_2 samples.

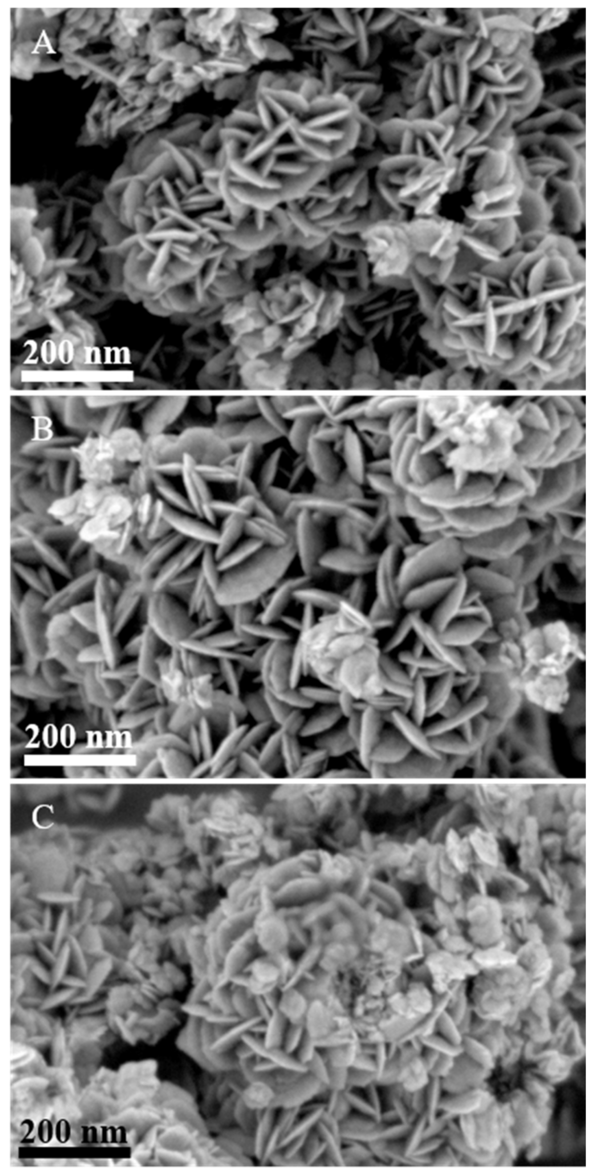

Fig. 2. SEM images of Cu-RM-A(A), Cu-RM-B(B), and Cu-RM-C(C).

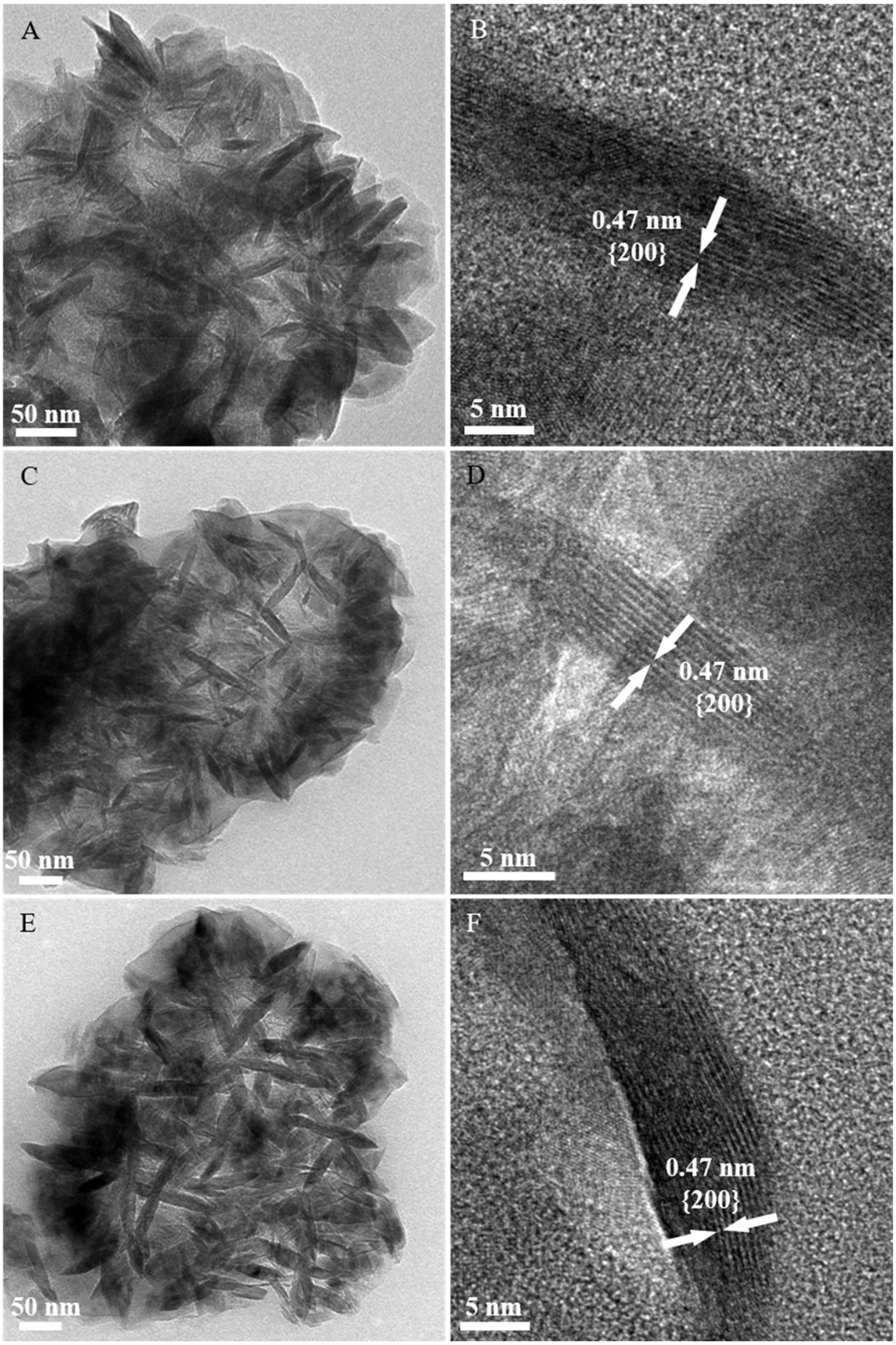

Fig. 3. TEM and HRTEM images of Cu-RM-A (A, B), Cu-RM-B (C, D), and Cu-RM-C (E, F).

The valance state of Mn is determined by fitting their Mn 2p spectra. The Mn 2p peaks around 643.6 and 654.5 eV are attributed to the Mn $2p_{3/2}$ and Mn $2p_{1/2}$ of Mn^{4+}. The Mn 2p peaks around 641.8 and 653.3 eV are attributed to the $Mn2p_{3/2}$ and $Mn2p_{1/2}$ of Mn^{3+} [41–44]. No XPS peaks attributed to those of Mn^{2+} are observed. The Mn^{3+}/Mn^{4+} atomic ratio for the Cu doped ramsdellite samples is estimated by the Mn 2p spectra fitting. For Cu-RM-A with the lowest Cu/Mn molar ratio, its Mn^{3+}/Mn^{4+} atomic ratio is 1.64, which is almost same as that of pure ramsdellite MnO_2 (1.61) [34]. With the Cu/Mn molar ratio increasing from 0.0037 to 0.0076 and 0.0120, the Mn^{3+}/Mn^{4+} atomic ratio of Cu-RM-B and Cu-RM-C increases to 1.82, 2.08, respectively. The increase in the Mn^{3+}/Mn^{4+} atomic ratio with increasing the Cu doping amount is attributed to the substitution of Mn ions with high valence states (3+ or 4+) by Cu ions with low valence state (2+) to keep charge balance in the Cu ion doped ramsdellite MnO_2 samples. According to the Mn^{3+}/Mn^{4+} atomic ratio, the average oxidation state (AOS) of Mn in Cu-RM-A, Cu-RM-B, and Cu-RM-C is calculated to be 3.38, 3.35, 3.32, respectively (Table 1).

The AOS of Mn in the Cu doped ramsdellite MnO_2 samples is also determined by analyzing the Mn3 s multiplet splitting magnitude (ΔE_s) according to the equation as follows [42,43]:

$$AOS = 8.95 - 1.13\,\Delta E_s \text{ (eV)}$$

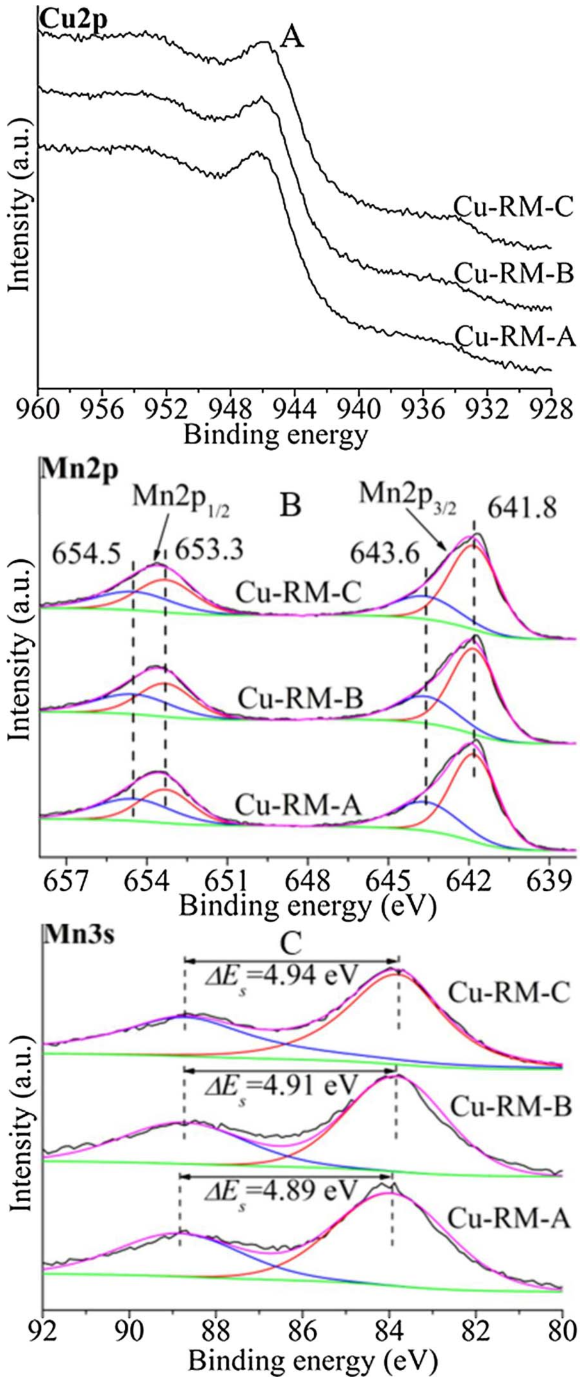

Fig. 4. Cu2p (A), Mn2p (B), and Mn3s (C) XPS spectra of the Cu doped ramsdellite MnO_2 samples.

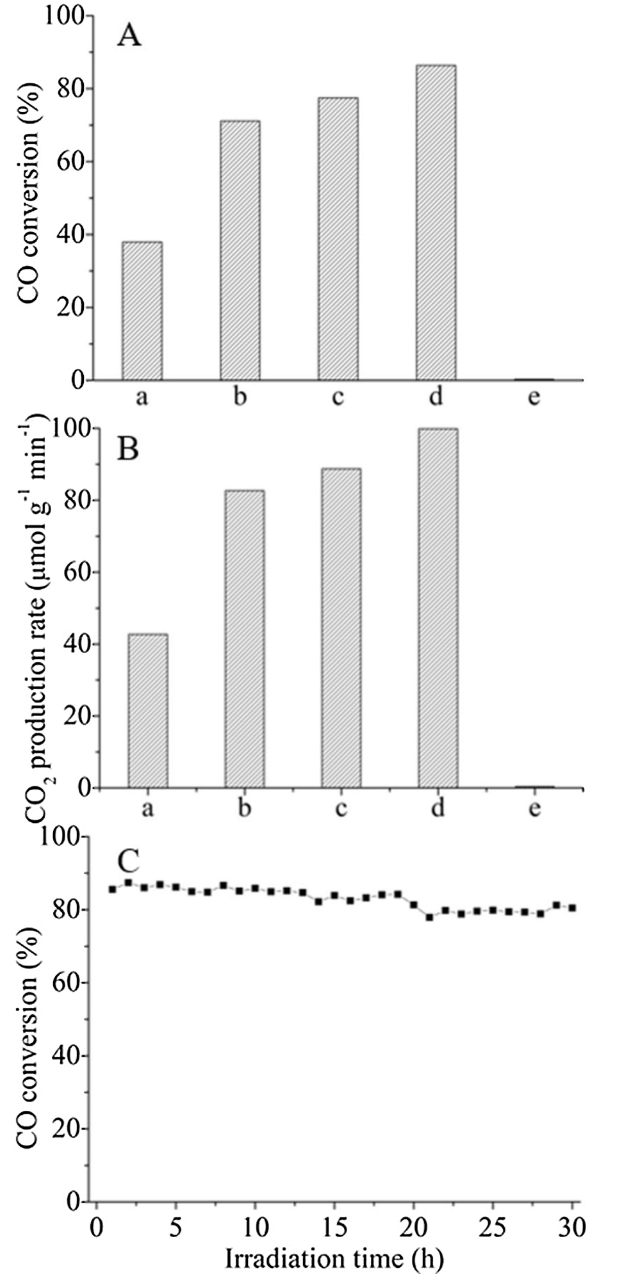

Fig. 5. CO conversion (A) and CO_2 production rate (B) of the samples, and photothermocatalytic stability of Cu-RM-C for CO oxidation (C) under the full solar spectrum irradiation: R-MnO_2 (a), Cu-RM-A(b), Cu-RM-B(c), Cu-RM-C(d), and TiO_2(P25)(e).

The ΔE_s of Cu-RM-A, Cu-RM-B, and Cu-RM-C is 4.69, 4.73, and 4.79 eV respectively. Their corresponding AOS is calculated to be 3.42, 3.40, and 3.37 respectively. The AOS value is in general accordance to the corresponding value obtained by analyzing Mn 2p spectra.

3.2. Photothermocatalytic activity

We measured the photothermocatalytic activity of the pure ramsdellite MnO_2 and Cu doped ramsdellite MnO_2 samples for the catalytic oxidation of CO as one of poisonous air pollutants under steady state with the irradiation of the Xe lamp, which has spectral profile similar to solar light [27]. Under the full solar spectrum irradiation with light intensity of 102.0 mW cm^{-2} (corresponding to ~1 sun), no CO is oxidized to CO_2 in the absence of catalyst (Fig. S2). R-MnO_2 has the lowest photothermocatalytic activity. Its CO conversion is only 37.9% (Fig. 5A) and its CO_2 production rate is 42.7 μmol $g^{-1}min^{-1}$ (Fig. 5B). The Cu doping significantly promotes its photothermocatalytic activity. Compared to R-MnO_2, the CO conversion and CO_2 production rate of Cu-RM-A with the Cu/Mn molar ratio of 0.0037 considerably increase to 71.1%, 82.7 μmol $g^{-1}min^{-1}$, respectively. With the Cu/Mn molar ratio increasing to 0.0076, the CO conversion and CO_2 production rate of Cu-RM-B increase to 77.5%, 88.8 μmol $g^{-1}min^{-1}$, respectively. Cu-RM-C with the Cu/Mn molar ratio of 0.0120 exhibits the highest catalytic activity. Its CO conversion increases to 86.4%. Its CO_2 production rate increase to 99.9 μmol $g^{-1}min^{-1}$, which is 2.3 times higher than that of R-MnO_2.

TiO_2 (P25) is a well-known benchmark photocatalyst for the photocatalytic purification of various water and air pollutants. It was

reported that TiO_2 exhibits photocatalytic activity for CO oxidation [45,46]. In order to make comparison, we measured the photocatalytic activity of TiO_2 (P25) for CO oxidation under the full solar spectrum irradiation. Under the same reaction condition as that of the Cu doped ramsdellite MnO_2 samples, TiO_2 (P25) demonstrates much lower photocatalytic activity. Its CO conversion is very low (0.3%). The CO_2 production rate of TiO_2 is only 0.35 μmol $g^{-1}min^{-1}$, which is 281.7 times lower than that of Cu-RM-C.

The photothermocatalytic stability of Cu-RM-C for CO oxidation under the full solar spectrum irradiation is investigated. As shown in Fig. 5C, at the initial one hour, the CO conversion is 85.6%. After continuously reacted for 30 h, the CO conversion is 80.5%. The result indicates that Cu-RM-C demonstrates very good catalytic stability.

The photothermocatalytic activity of Cu-RM-C for CO oxidation in the different flow rate of the feed stream with 15 g m^{-3} of CO (produced by mixing 5 vol% CO/He and 20.8 vol% O_2/N_2) under the full solar spectrum irradiation was measured. With the flow rate of the feed stream increasing from 20 (Fig. 5) to 30, 36, and 47 mL min^{-1} (the corresponding space velocity is 12000, 18000, 21600, and 28200 mL g^{-1} h^{-1}), CO conversion decreases from 86.4 to 72.8, 69.5, 57.4% while the CO_2 production rate increases from 99.9 to 118.8, 131.7, 146.1 μmol $g^{-1}min^{-1}$, respectively (Fig. S3).

The photothermocatalytic activity of Cu-RM-C for CO oxidation under the irradiation of visible-infrared or infrared light was measured. Under the visible-infrared irradiation of $\lambda > 420$, 480, 560, or 690 nm, its CO conversion is 79.6%, 77.4%, 73.4%, 71.0%, respectively (Fig. 6A). The corresponding CO_2 production rate is 94.1, 91.3, 85.1, 82.7 μmol g^{-1} min^{-1}, respectively (Fig. 6B). Even under the $\lambda > 830$ nm infrared irradiation, Cu-RM-C still demonstrates very good photothermocatalytic activity with 68.2% of CO conversion and 78.4 μmol g^{-1} min^{-1} of CO_2 production rate. The result indicates that Cu-RM-C demonstrates very good photothermocatalytic activity for CO oxidation under the visible-infrared or infrared irradiation.

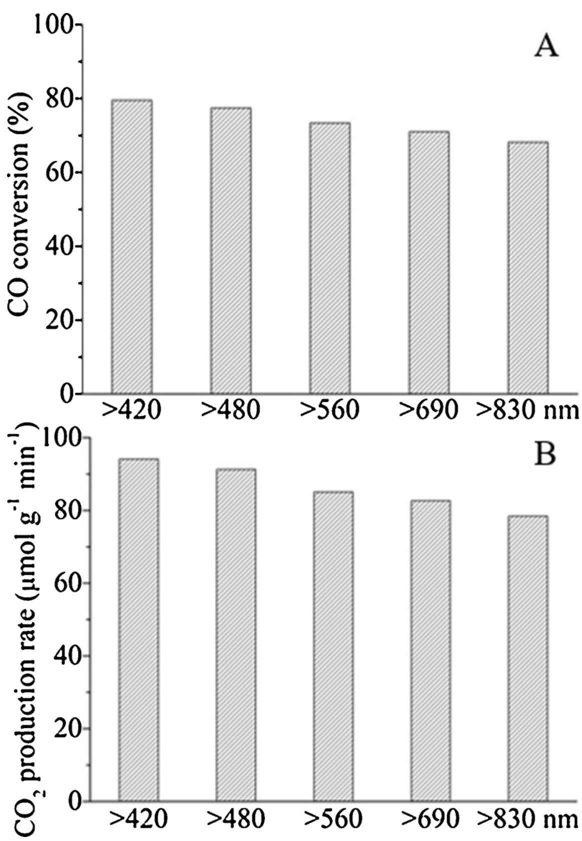

Fig. 6. CO conversion (A) and CO_2 production rate (B) of Cu-RM-C for CO oxidation under the visible-infrared or infrared irradiation.

3.3. Mechanism

Why does the Cu-RM-C sample demonstrate very good photothermocatalytic activity for CO oxidation under the irradiation of the Xe lamp? To address the issue, we measure its optical absorption as it is essential to a photocatalytic process. For comparison, the optical absorption of R-MnO_2 is also measured. As shown in Fig. 7A, the Cu-RM-C sample demonstrate strong optical absorption across the entire solar spectrum region (200 ~ 2400 nm). Compared with Cu-RM-C, R-MnO_2 has a relatively lower absorption in the region of $\lambda > 650$ nm, indicating that the Cu doping alters the optical property of ramsdellite MnO_2.

Does the strong optical absorption of the Cu doped ramsdellite MnO_2 sample cause conventional photocatalysis like TiO_2? To address the issue, we measure the photocatalytic activity of Cu-RM-C for CO oxidation at near ambient temperature under the full solar spectrum irradiation (Experimental). In this case, the photocatalytic activity of Cu-RM-C is very low (Fig. 7B). This result suggests that the very high catalytic activity of Cu-RM-C under the full solar spectrum irradiation (Fig. 5) mainly derives from solar-light-driven thermocatalysis rather than the conventional photocatalysis: The strong optical absorption of Cu-RM-C causes an increase in its temperature. When the temperature exceeds the light-off temperature ($T_{light\text{-}off}$) of the thermocatalytic oxidation of CO on Cu-RM-C, the thermocatalytic reaction proceeds.

To affirm this mechanism, we measure the surface temperature of the Cu-RM-C sample during the catalytic reaction of CO oxidation under the irradiation of the Xe lamp (Fig. 5A). Under the full solar spectrum irradiation, the temperature of Cu-RM-C quickly reaches an equilibrium temperature (T_{eq}) of 120 °C (Fig. 7C), indicating that Cu-RM-C efficiently converts the absorbed solar energy to the thermal energy. The T_{eq} of Cu-RM-C is slightly higher than that of R-MnO_2 (113 °C), which is attributed to the stronger optical absorption of Cu-RM-C in the region of $\lambda > 650$ nm than the latter (Fig. 7A). The T_{eq} of Cu-RM-C under the visible-infrared or infrared irradiation is also measured. The T_{eq} of Cu-RM-C under the visible-infrared or infrared irradiation of $\lambda > 420$, 480, 560, 690, and 830 nm is 118, 116, 114, 112, 110 °C, respectively. We also measured the corresponding air temperature in the reactor in the presence of the Cu-RM-C sample under the irradiation of the Xe lamp. Under the full solar spectrum, and visible-infrared or infrared irradiation of $\lambda > 420$, 480, 560, 690, and 830 nm, the corresponding air temperature is 56, 54, 53, 51, 50, and 48 °C, respectively (Fig. S4). The air temperature increase is due to the heating effect by the infrared irradiation from the Xe lamp. The result indicates that the Cu doped ramsdellite sample efficiently converts the absorbed visible-infrared or infrared energy to thermal energy.

Does the T_{eq} of Cu-RM-C reach to its $T_{ligh\text{-}off}$ for CO oxidation? To address the issue, the thermocatalytic activity of Cu-RM-C for CO oxidation at different temperature in the dark is measured (Experimental). As shown in Fig. 7D, Cu-RM-C demonstrates very good thermocatalytic activity. Even at near room temperature (40 °C), CO starts to be oxidized to CO_2 ($T_{ligh\text{-}off} = \sim 40$ °C). When the reaction temperature increases from 80 to 160 °C, the thermocatalytic activity of Cu-RM-C is significantly enhanced. Its T_{50} and T_{90} (corresponding to the temperature of 50% and 90% CO conversion) are 124, 157 °C respectively. All the T_{eq} of Cu-RM-C under the irradiation of full solar spectrum, visible-infrared, or infrared light is higher than its $T_{ligh\text{-}off}$. Therefore, the solar-light-driven thermocatalytic CO oxidation can proceed.

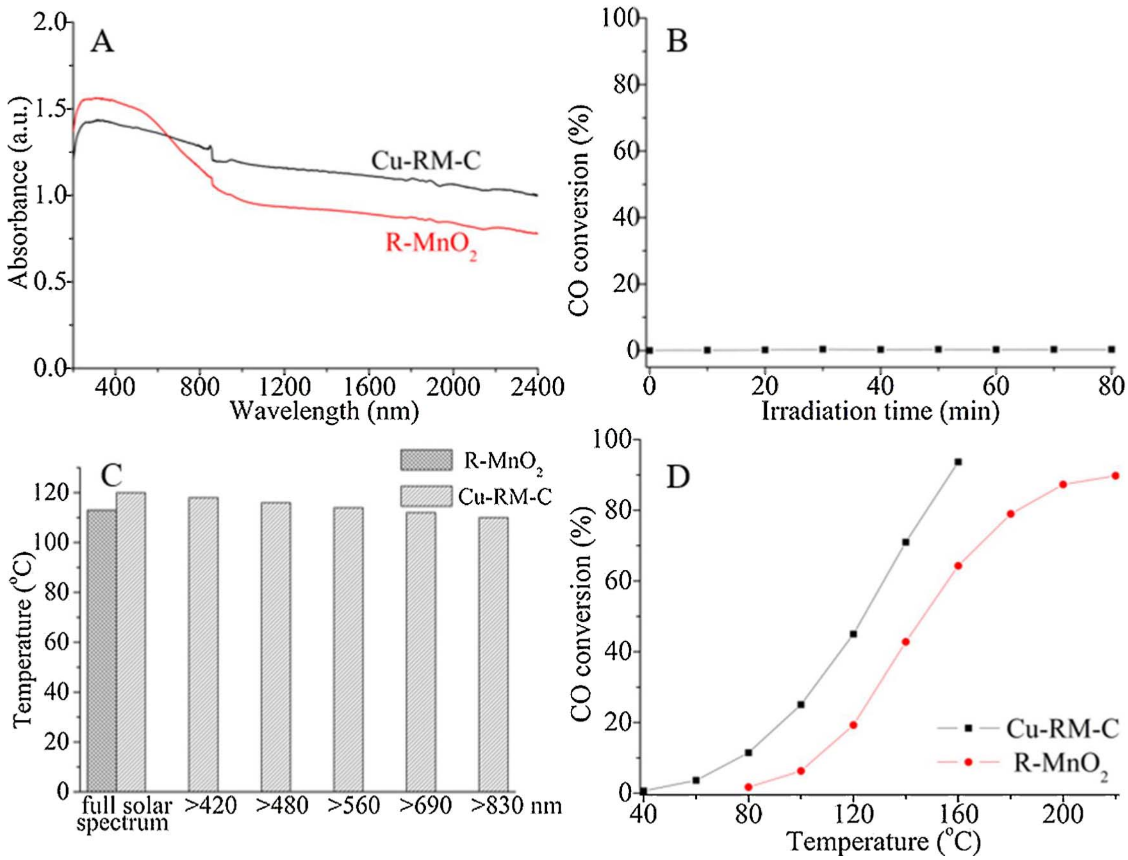

Fig. 7. Reflectance diffusive absorption of $R\text{-}MnO_2$ and Cu-RM-C (A); Photocatalytic activity of Cu-RM-C for CO oxidation at near room temperature (B); Equilibrium temperature of MnO_2 and Cu-RM-C under the irradiation of full solar spectrum, visible-infrared, or infrared light (C); Thermocatalytic activity of MnO_2 and Cu-RM-C for CO oxidation at different temperature in the dark (D).

Why does Cu-RM-C demonstrate much higher phototherocatalytic activity than $R\text{-}MnO_2$ (Fig. 5A and B)? To address the issue, we also measure the thermocatalytic activity of $R\text{-}MnO_2$ for CO oxidation at different temperature in the dark. As shown in Fig. 7D, $R\text{-}MnO_2$ demonstrates much lower thermocatalytic activity as compared to Cu-RM-C. Its T_{50} and T_{90} are 147, 220 °C, respectively. Compared to $R\text{-}MnO_2$, the T_{50} and T_{90} of Cu-RM-C are reduced by 23, 63 °C, respectively. The much higher thermocatalytic activity of Cu-RM-C than $R\text{-}MnO_2$ together with its more efficient photothermal conversion (Fig. 7A–D) results in its much higher photothermocatalytic activity under the full solar spectrum irradiation (Fig. 5A and B).

3.4. Origin of the enhanced thermocatalytic activity

It is well-known that thermocatalytic oxidation on manganese oxide proceeds according to Mars – van Krevelen redox mechanism [41–43]: reductant (e.g. CO in the present case) is oxidized by the surface lattice oxygen of manganese oxide, and then the resultant oxygen vacancies are refilled by O_2. It is widely accepted that the thermocatalytic oxidation activity of manganese oxide is mainly decided by its lattice oxygen activity because the reduction of manganese oxide is sluggish as compared to the replenishment of the formed oxygen vacancies [41–43]. Therefore, to address the issue why the Cu doping causes the considerable enhancement of thermocatalytic activity of ramsdellite MnO_2, CO-TPR is used to investigate the effect of the Cu doping on the lattice oxygen activity of Cu-RM-C than $R\text{-}MnO_2$. As shown in Fig. 8A, compared to the CO-TPR profile of $R\text{-}MnO_2$, the corresponding CO consumption peaks of Cu-RM-C considerably shift to lower temperatures. This result reveals that the Cu doping considerably promotes the lattice oxygen activity of $R\text{-}MnO_2$, thus resulting in the enhancement of its thermocatalytic activity.

To provide more evidence, the effect of the Cu doping on the lattice oxygen activity of $R\text{-}MnO_2$ is theoretically investigated by DFT calculation. The energy (ΔE) of removing one lattice oxygen from $Mn_{32}O_{64}$ or $Mn_{31}CuO_{64}$ supercell with orthorhombic ramsdellite structure (Fig. 8B and C) is calculated:

$$Mn_{32}O_{64} = 0.5O_2 + Mn_{32}O_{63}$$

$$Mn_{31}CuO_{64} = 0.5O_2 + Mn_{31}CuO_{63}$$

$$\Delta E = E_{Mn32O63} + 0.5E_{O2} - E_{Mn32O64}$$

$$\Delta E = E_{Mn31CuO63} + 0.5E_{O2} - E_{Mn31CuO64}$$

The ΔE of removing type-I or type-II lattice oxygen from $Mn_{32}O_{64}$ supercell is 2.05, 2.43 eV, respectively. Compared to $Mn_{32}O_{64}$ supercell, the ΔE of removing type-I lattice oxygen (nearby the substituted Cu) from $Mn_{31}CuO_{64}$ supercell considerably decreases from 2.05 to 0.70 eV. The ΔE of removing type-II lattice oxygen from $Mn_{31}CuO_{64}$ supercell decreases from 2.43 to 2.02 eV (Fig. 8C). The DFT calculation reveals that the Cu doping considerably enhances the lattice oxygen activity of $R\text{-}MnO_2$, which is in accordance to the experimental result by CO-TPR.

3.5. Photoactivation

Does the highly efficient photothermocatalytic activity of Cu-RM-C under the full solar spectrum irradiation (Fig. 5) merely derive from the

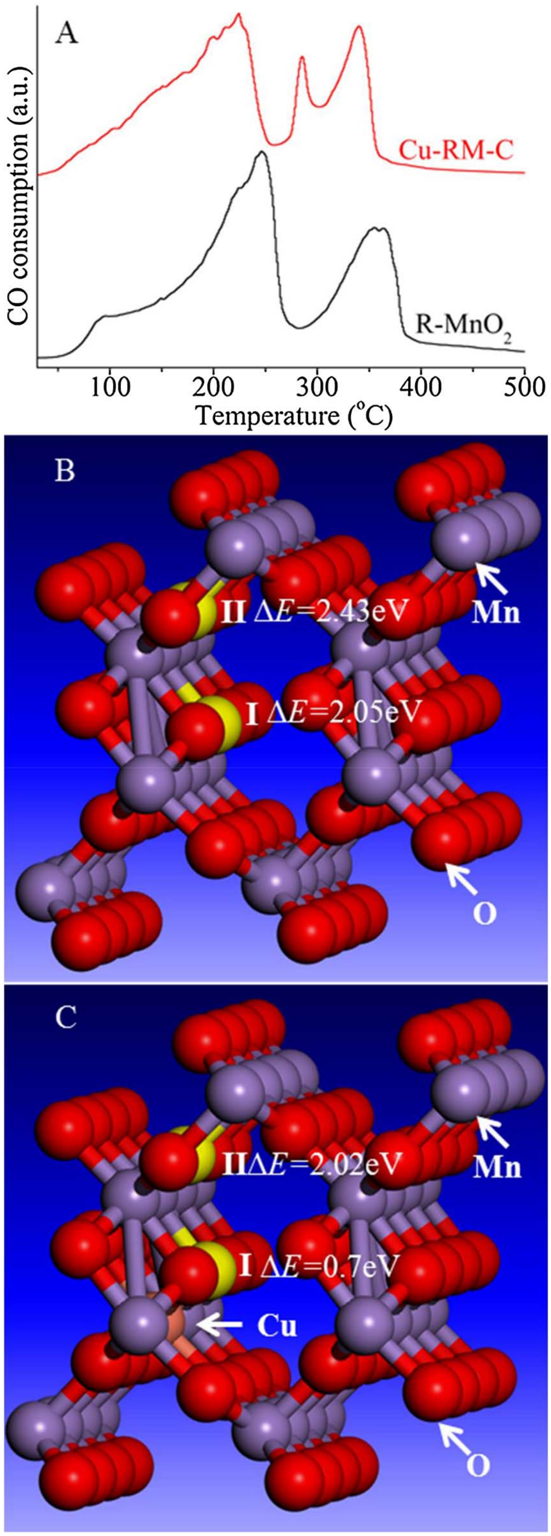

Fig. 8. CO-TPR profiles of R-MnO_2 and Cu-RM-C (A); ΔE of removing one lattice oxygen (yellow sphere) from super cells of $Mn_{32}O_{64}$ (B) and $Mn_{31}CuO_{64}$ (C) with orthorhombic ramsdellite structure. (For interpretation of the references to colour in this figure legend, the reader is referred to the web version of this article.)

solar-light-driven thermocatalysis? To clarify this issue, we measure the catalytic activity of Cu-RM-C for CO oxidation at different temperature in the dark or with the full solar spectrum irradiation under the otherwise identical reaction condition (Experimental). As shown in Fig. 9A, compared to the CO_2 production rate of Cu-RM-C in the dark, at the same temperature from 40 to 120 °C, the full solar spectrum irradiation causes an obvious enhancement in its catalytic activity. This result clearly demonstrates the presence of photoactivation for CO oxidation on Cu-RM-C under the full solar spectrum irradiation, which improves its solar-light-driven themocatalytic activity. As Cu-RM-C has no photocatalytic activity at near room temperature as shown in Fig. 7B, the novel photoactivation is completely unlike the well-known photoactivation of the redox reaction induced by photogenerated electrons and holes on photocatalytic semiconductors (e.g. TiO_2) which is able to proceed at room temperature [1,3].

As the thermocatalytic oxidation activity of manganese oxide is mainly decided by its lattice oxygen activity as discussed above, the effect of the irradiation on the lattice oxygen activity of Cu-RM-C is investigated to put more physical insight in the photoactivation (Experimental). Fig. 9B shows the CO-TPR profiles of Cu-RM-C in the dark or with the full solar spectrum irradiation. Compared to the CO-TPR profiles of Cu-RM-C in the dark, the full solar spectrum irradiation causes an obvious shift of the CO consumption peaks to lower temperatures. The result suggests that the full solar spectrum irradiation promotes the lattice oxygen activity of Cu-RM-C, thus promoting its solar-light-driven thermocatalytic activity.

To provide more evidence to the novel photoactivation, the effect of the irradiation on the lattice oxygen activity of Cu-RM-C is theoretically investigated by DFT calculation. The irradiation on manganese oxide causes *d-d* transition (t_{2g}-e_g) of Mn ions in the octahedral sites [47,48], which results in the change in the number of electrons in up and down spin component for manganese oxide. The ΔE of removing one lattice oxygen from $Mn_{31}CuO_{64}$ supercell with orthorhombic ramsdellite structure in excited state (Fig. 9C) is calculated by a constrained occupancy approach of DFT through setting the excitation of one *d* electron to the excited state by changing the electron number of up and down spin component [49,25].

$$Mn_{31}CuO_{64}^{*}\ (\text{excited}) = 0.5O_2 + Mn_{31}CuO_{63}^{*}(\text{excited})$$

$$\Delta E = E_{Mn31CuO63^*} + 0.5E_{O2} - E_{Mn31CuO64^*}$$

Compared to the corresponding ΔE value in the ground state, the ΔE of removing type-I lattice oxygen from $Mn_{31}CuO_{64}$ supercell in the excited state reduces from 0.70 to 0.58 eV. The ΔE of removing type-II lattice oxygen from $Mn_{31}CuO_{64}$ supercell considerably reduces from 2.02 to 1.68 eV (Fig. 9C). The DFT calculation reveals that the irradiation enhances the lattice oxygen activity of $Mn_{31}CuO_{64}$, which is in accordance to the experimental result by CO-TPR.

4. Conclusion

In summary, the Cu doped ramsdellite MnO_2 nanosheets with different Cu/Mn molar ratio were prepared by a facile hydrothermal redox reaction among $Cu(NO_3)_2$, $Mn(NO_3)_2$, and $KMnO_4$. The Cu doped ramsdellite MnO_2 nanosheet samples demonstrate much higher catalytic activity than the pure ramsdellite MnO_2 nanosheets and very good catalytic stability for CO oxidation under the full solar spectrum irradiation. The Cu doped ramsdellite MnO_2 nanosheet sample also demonstrates highly efficient catalytic activity for CO oxidation even under the $\lambda > 830$ nm infrared irradiation. The highly efficient catalytic activity of the Cu doped ramsdellite MnO_2 nanosheet sample derives from efficient solar-light-driven thermocatalysis because of its strong absorption across the entire full solar spectrum and high thermocatalytic activity. The Cu doping considerably enhances the lattice oxygen activity of ramsdellite MnO_2, thus promoting its thermocatalytic activity. A novel photoactivation, completely unlike the well-known photocatalysis on photocatalytic semiconductors such as TiO_2, is discovered to further promote the solar-light-driven thermocatalytic activity. The present work provides highly efficient material and energy-saving strategy for the purification of CO as one of poisonous air pollutants by using renewable solar energy.

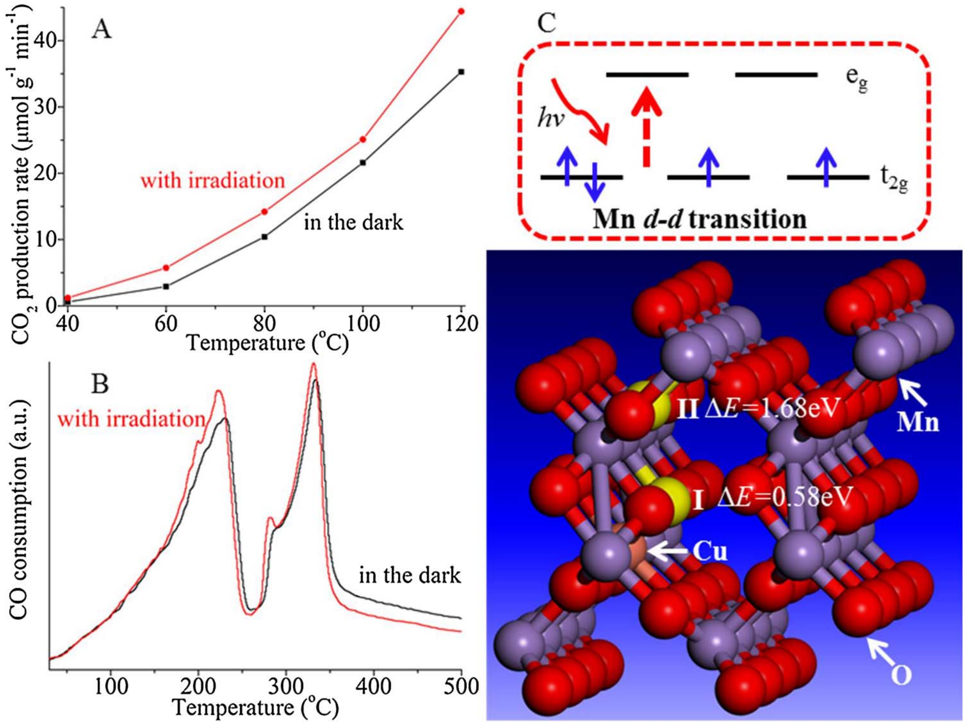

Fig. 9. The catalytic activity of Cu-RM-C for CO oxidation at the different temperature (A) and CO-TPR profile of Cu-RM-C (B) in the dark or with the full solar spectrum irradiation; The ΔE of removing one lattice oxygen (yellow sphere) from $Mn_{31}CuO_{64}$ supercell with ramsdellite structure in excited state (C). (For interpretation of the references to colour in this figure legend, the reader is referred to the web version of this article.)

Acknowledgements

This work was supported by National Natural Science Foundation of China (21473127, 21673168).

Appendix A. Supplementary data

Supplementary data associated with this article can be found, in the online version, at http://dx.doi.org/10.1016/j.apcatb.2017.11.017.

References

[1] X.B. Chen, S.S. Mao, Chem. Rev. 107 (2007) 2891–2959.
[2] A. Kubacka, M. Fernandez-Garcia, G. Colon, Chem. Rev. 112 (2011) 1555–1614.
[3] L. Ren, Y.Z. Li, J.T. Hou, J.L. Bai, M.Y. Mao, M. Zeng, X.J. Zhao, Appl. Catal. B 181 (2016) 625–634.
[4] Y.H. Sang, H. Liu, A. Umar, Chemcatchem 7 (2015) 559–573.
[5] J. Tian, Y.H. Sang, G.W. Yu, H.D. Jiang, X.N. Mu, H. Liu, Adv. Mater. 25 (2013) 5075–5080.
[6] Z.J. Zhang, W.Z. Wang, Dalton. Trans. 42 (2013) 12072–12074.
[7] J. Tao, D. Ying, W. Wei, X.C. Ma, B.B. Huang, Phys. Chem. Chem. Phys. 16 (2014) 18596–18604.
[8] G. Wang, B.B. Huang, X.C. Ma, Z.Y. Wang, X.Y. Qin, X.Y. Zhang, Y. Dai, M.H. Whangbo, Angew. Chem. Int. Ed. 52 (2013) 1–5.
[9] Z.J. Li, Y. Dai, X.C. Ma, Y.T. Zhu, B.B. Huang, Phys. Chem. Chem. Phys. 16 (2014) 3267–3273.
[10] Y.H. Sang, Z.H. Zhao, M.W. Zhao, P. Hao, Y.H. Leng, H. Liu, Adv. Mater. 27 (2015) 363–369.
[11] C. Pak, J.Y. Woo, K. Lee, W.D. Kim, Y. Yoo, D.C. Lee, J. Phys. Chem. C 116 (2012) 25407–25414.
[12] W. Jiang, X.Y. Wang, Z.M. Wu, X.N. Yue, S.J. Yuan, H.F. Lu, B. Liang, Ind. Eng. Chem. Res. 54 (2015) 832–841.
[13] C.H. Li, F. Wang, J. Zhu, J.C. Yu, Appl. Catal. B 100 (2010) 433–439.
[14] W.P. Qin, D.S. Zhang, D. Zhao, L.L. Wang, K.Z. Zheng, Chem. Commun. 46 (2010) 2304–2306.
[15] Z.X. Li, F.B. Shi, T. Zhang, H.S. Wu, L.D. Sun, C.H. Yan, Chem. Commun. 47 (2011) 8109–8111.
[16] S.Q. Huang, L. Gu, C. Miao, Z.Y. Lou, N.W. Zhu, H.P. Yuan, A.D. Shan, J. Mater. Chem. A 1 (2013) 7874.
[17] W. Wang, W.J. Huang, Y.R. Ni, C.H. Lu, Z.Z. Xu, ACS Appl. Mater. Interfaces 6 (2014) 340–348.
[18] J. Tian, Y.H. Leng, Z.H. Zhao, Y. Xia, Y.H. Sang, P. Hao, J. Zhan, M.C. Li, H. Liu, Nano Energy 11 (2015) 419–427.
[19] H.T. Li, R.H. Liu, Y. Liu, H. Huang, H. Yu, H. Ming, S.Y. Lian, S.T. Lee, Z.H. Kang, J. Mater. Chem. 22 (2012) 17470.
[20] J.B. Cui, Y.J. Li, L. Liu, L. Chen, J. Xu, J.W. Ma, G. Fang, E.B. Zhu, H. Wu, L.X. Zhao, L.Y. Wang, Y. Huang, Nano Lett. 15 (2015) 6295–6301.
[21] W.Y. Jiang, S. Bai, L.M. Wang, X.J. Wang, L. Yang, Y.R. Li, D. Liu, X.N. Wang, Z.Q. Li, J. Jiang, Y.J. Xiong, Small 12 (12) (2016) 1640–1648.
[22] Z.K. Zheng, T. Tachikawa, T. Majima, J. Am. Chem. Soc. 136 (2014) 6870–6873.
[23] R.Y. Yan, M. Chen, H. Zhou, T. Liu, X.W. Tang, K. Zhang, H.X. Zhu, J.H. Ye, D. Zhang, T.X. Fan, Sci. Rep. 6 (2016) 20001.
[24] M.Y. Mao, Y.Z. Li, J.T. Hou, M. Zeng, X.J. Zhao, Appl. Catal B 174 (2015) 496–503.
[25] F. Liu, M. Zeng, Y.Z. Li, Y. Yang, M.Y. Mao, X.J. Zhao, Adv. Funct. Mater. 26 (2016) 4518–4526.
[26] Y. Ma, Y.Z. Li, M.Y. Mao, J.T. Hou, M. Zeng, X.J. Zhao, J. Mater. Chem. A 3 (2015) 5509–5516.
[27] J.T. Hou, Y.Z. Li, M.Y. Mao, Y.Z. Yue, G.N. Greaves, X.J. Zhao, Nanoscale 7 (2015) 2633–2640.
[28] H.H. Liu, Y.Z. Li, Y. Yang, M.Y. Mao, M. Zeng, L. Lan, L. Yun, X.J. Zhao, J. Mater. Chem. A 4 (2016) 9890–9899.
[29] D. Jiang, W.Z. Wang, L. Zhang, R.H. Qiu, S.M. Sun, Y.L. Zheng, Appl. Catal. B 165 (2015) 399–407.
[30] D. Jiang, W.Z. Wang, E. Gao, L. Zhang, S.M. Sun, J. Phys. Chem. C 117 (2013) 24242–24249.
[31] Y.L. Zheng, W.Z. Wang, D. Jiang, L. Zhang, X.M. Li, Z. Wang, J. Mater. Chem. A 4 (2016) 105–112.
[32] J.L. Fang, D.Z. Li, Y. Shao, J.H. Hu, J. Mater. Chem. A 4 (2016) 14213–14221.
[33] M.Y. Mao, Y.Z. Li, H.Q. Lv, J.T. Hou, M. Zeng, L. Ren, H. Huang, X.J. Zhao, Environ. Sci. Nano 4 (2017) 373–384.
[34] Y. Yang, Y.Z. Li, M.Y. Mao, M. Zeng, X.J. Zhao, ACS Appl. Mater. Interfaces 9 (2017) 2350–2357.
[35] M. Zeng, Y.Z. Li, F. Liu, Y. Yang, M.Y. Mao, X.J. Zhao, Appl. Catal. B 200 (2017) 521–529.
[36] P.E. Blochl, Phys. Rev. B 50 (1994) 17953.
[37] G. Kresse, J. Hafner, Phys. Rev. B 48 (1993) 13115.
[38] C.H. Sun, Y. Wang, J. Zou, S.C. Smith, Phys. Chem. Chem. Phys. 13 (2011) 11325–11328.
[39] G. Wang, B.B. Huang, X.C. Ma, Z.Y. Wang, X.Y. Qin, X.Y. Zhang, Y. Dai, M.H. Whangbo, Angew. Chem. Int. Ed. 52 (2013) 4810–4813.
[40] S. Poulston, P.M. Parlett, P. Stone, M. Bowker, Surf. Interface Anal. 24 (1996) 811–820.
[41] J.T. Hou, L.L. Liu, Y.Z. Li, M.Y. Mao, H.Q. Lv, X.J. Zhao, Environ. Sci. Technol. 47 (2013) 13730–13736.
[42] J.T. Hou, Y.Z. Li, M.Y. Mao, L. Ren, X.J. Zhao, ACS Appl. Mater. Interfaces 6 (2014) 14981–14987.

[43] V.P. Santos, O.S.G.P. Soares, J.J.W. Bakker, M.F.R. Pereira, J.J.M. Orfao, J. Gascon, F. Kapteijn, J.L. Figueiredo, J. Catal. 293 (2012) 165–174.
[44] H.C. Genuino, S. Dharmarathna, E.C. Njagi, M.C. Mei, S.L. Suib, J. Phys. Chem. C 116 (2012) 12066–12078.
[45] W.X. Dai, X. Chen, X.P. Zheng, Z.Z. Ding, X.X. Wang, P. Liu, X.Z. Fu, ChemPhysChem 10 (2009) 411–419.
[46] S. Hwang, M.C. Lee, W. Choi, Appl. Catal. B 46 (2003) 49–63.
[47] N. Sakai, Y. Ebina, K. Takada, T. Sasaki, J. Phys. Chem. B 109 (2005) 9651–9655.
[48] Y.K. Hsu, Y.C. Chen, Y.G. Lin, L.C. Chen, K.H. Chen, J. Mater. Chem. 22 (2012) 2733–2739.
[49] A. Canning, A. Chaudhry, R. Boutchko, N. Gronbech-Jensen, Phys. Rev. B 83 (2011) 125115.